HHS Public Access

Author manuscript

Glia. Author manuscript; available in PMC 2019 March 01.

Published in final edited form as:

Glia. 2019 March ; 67(3): 452–466. doi:10.1002/glia.23555.

Astrocyte progenitor transplantation promotes regeneration of bulbospinal respiratory axons, recovery of diaphragm function, and a reduced macrophage response following cervical spinal cord injury

Miguel Goulão[1,2], **Biswarup Ghosh**[1], **Mark W. Urban**[1], **Malya Sahu**[1], **Christina Mercogliano**[1], **Brittany A. Charsar**[1], **Sreeya Komaravolu**[1], **Cole G. Block**[1], **George M. Smith**[3], **Megan C. Wright**[4], and **Angelo C. Lepore**[1]

[1]Department of Neuroscience, Vickie and Jack Farber Institute for Neuroscience, Sidney Kimmel Medical College at Thomas Jefferson University, Philadelphia, Pennsylvania

[2]Life and Health Sciences Research Institute (ICVS), School of Medicine, ICVS/3B's - PT Government Associate Laborator, University of Minho, Braga, Portugal

[3]Department of Neuroscience, Shriners Hospitals Pediatric Research Center, Temple University School of Medicine, Philadelphia, Pennsylvania

[4]Department of Biology, Arcadia University, Glenside, Pennsylvania

Abstract

Stem/progenitor cell transplantation delivery of astrocytes is a potentially powerful strategy for spinal cord injury (SCI). Axon extension into SCI lesions that occur spontaneously or in response to experimental manipulations is often observed along endogenous astrocyte "bridges," suggesting that augmenting this response via astrocyte lineage transplantation can enhance axon regrowth. Given the importance of respiratory dysfunction post-SCI, we transplanted glial-restricted precursors (GRPs)—a class of lineage-restricted astrocyte progenitors—into the C2 hemisection model and evaluated effects on diaphragm function and the growth response of descending rostral ventral respiratory group (rVRG) axons that innervate phrenic motor neurons (PhMNs). GRPs survived long term and efficiently differentiated into astrocytes in injured spinal cord. GRPs promoted significant recovery of diaphragm electromyography amplitudes and stimulated robust regeneration of injured rVRG axons. Although rVRG fibers extended across the lesion, no regrowing axons re-entered caudal spinal cord to reinnervate PhMNs, suggesting that this regeneration response—although impressive—was not responsible for recovery. Within ipsilateral C3–5 ventral horn (PhMN location), GRPs induced substantial sprouting of spared fibers originating in contralateral rVRG and 5-HT axons that are important for regulating PhMN excitability; this sprouting was likely involved in functional effects of GRPs. Finally, GRPs reduced the macrophage response (which plays a key role in inducing axon retraction and limiting

Correspondence: Angelo C. Lepore, Ph.D. Department of Neuroscience, Vickie and Jack Farber Institute for Neurosciences, Sidney Kimmel Medical College at Thomas Jefferson University, 900 Walnut Street, JHN 469, Philadelphia, PA 19107. angelo.lepore@jefferson.edu.

CONFLICT OF INTEREST

The authors declare no competing financial interests.

regrowth) both within the hemisection and at intact caudal spinal cord surrounding PhMNs. These findings demonstrate that astrocyte progenitor transplantation promotes significant plasticity of rVRG-PhMN circuitry and restoration of diaphragm function and suggest that these effects may be in part through immunomodulation.

Keywords

5-HT; breathing; GRP; phrenic motor neurons; regrowth; SCI; sprouting; stem cell

1 | INTRODUCTION

1.1 | Respiratory dysfunction is a major problem following SCI

Pulmonary compromise is a leading cause of mortality and morbidity after SCI, both acutely and at chronic stages (Shanmuganathan, Gullapalli, Zhuo, & Mirvis, 2008). There is decreased life expectancy for ventilator-dependent patients, often due to respiratory infections. Limited spontaneous respiratory recovery can occur after SCI; however, this response is often insufficient to allow individuals to regain significant breathing function or to perform other important pulmonary tasks such as coughing (which can result in respiratory infection) (Warren & Alilain, 2014). Importantly, cervical SCI represents greater than half of all human cases, in addition to often resulting in the most severe physical and psychological debilitation (Lane, Fuller, White, & Reier, 2008a). Cervical trauma disrupts the critical neural circuitry that controls a number of respiratory muscles, in particular the diaphragm (Warren, Awad, & Alilain, 2014).

1.2 | Diaphragm dysfunction plays a central role in respiratory compromise after cervical SCI

Compromise in inspiratory breathing occurs in a significant percentage of SCI patients due to paralysis of the major inspiratory muscle, the diaphragm (but likely also via effects on other muscles) (Strakowski, Pease, & Johnson, 2007). The diaphragm is innervated by PhMNs located at cervical levels 3–5 (Lane, Lee, Fuller, & Reier, 2009). PhMN output is driven by descending premotor bulbospinal neurons in the rostral ventral respiratory group (rVRG) of the medulla (Zimmer, Nantwi, & Goshgarian, 2007). Cervical SCI results in diaphragmatic respiratory compromise due to (a) PhMN loss and/or (b) injury to descending bulbospinal respiratory axonal projections and consequent silencing of spared PhMNs.

1.3 | Little-to-no axon regrowth occurs post-SCI

A number of mechanisms limit/prevent a robust axon regrowth response and ultimately the synaptic reconnectivity that will mediate functional restoration. These include (a) neuronal-intrinsic factors that limit ability of both injured and spared CNS neurons to mount a regenerative response (Luo & Park, 2012), (b) environmental impediments to axon growth such as an acellular cystic cavity, the physical and molecular barrier presented by the glial scar, myelin-associated inhibitory molecules, and repulsive developmental axon guidance molecules that continue to be expressed in the adult nervous system (Giger, Hollis, &

Tuszynski, 2010) (Bradbury et al., 2002); and (c) a lack of guidance cues to direct axons back to their correct neuronal targets (Harvey et al., 2015).

1.4 | Transplantation of astrocyte progenitors or more mature cells of the astroglial lineage is potentially powerful—yet relatively unexplored—strategy for the treatment of SCI

Astrocyte-mediated mechanisms that may be capable of promoting regeneration of damaged axons and sprouting of spared fibers include (a) providing a cellular substrate for axonal extension in the cystic lesion; (b) provision of beneficial molecules such as neurotrophins (Davies et al., 2006; Haas, Neuhuber, Yamagami, Rao, & Fischer, 2012; Hamby & Sofroniew, 2010; Hill et al., 2004); (c) production of extracellular matrix and cell adhesion molecules (Falnikar, Li, & Lepore, 2015); and (d) immunomodulation (Sofroniew, 2015).

Large, cystic lesions (which are characteristic of human SCI [Norenberg, Smith, & Marcillo, 2004]) provide minimal-to-no substrate for allowing robust axon regrowth, even if neuronal-intrinsic and extrinsic inhibitory mechanisms such as phosphatase and tensin homolog (PTEN) and chondroitin sulfate proteoglycans (CSPGs), respectively, are successfully antagonized. Interestingly, axonal growth into these SCI lesions that occurs spontaneously or in response to experimental manipulations often occurs along “bridges” of endogenous growth-promoting astrocytes (Zukor et al., 2013), suggesting that augmenting this astrocyte response via astrocyte lineage transplantation can enhance axonal regrowth.

1.5 | Macrophage contribution to axon growth inhibition

Resident microglia- and peripheral hematogenous monocyte-derived macrophages play key roles in inducing axonal retraction and limiting axon regrowth after SCI (Silver, Schwab, & Popovich, 2015). Both populations are macrophages within the CNS. Microglia are the earliest responders to insults such as SCI and peripheral nerve damage (Graeber & Christie, 2012). The microglial response includes upregulation of genes such as Iba1 and ED1/CD68, a morphological shift from a ramified/resting to an ameboidal/effector state, and production of a host of pro-inflammatory molecules (Calvo & Bennett, 2012). The microglial response is followed by infiltration of peripheral leukocytes, in particular hematogenous macrophages that can profoundly alter neuron and glia properties (Clark, Old, & Malcangio, 2013). Astrocytes normally form borders to restrict immune cell (including macrophages) entry into CNS parenchyma at blood–brain barrier and meninges in intact CNS and at glial scar sites after injury (Sofroniew, 2015). Astrocytes also can dampen the inflammatory phenotype of microglia/macrophage via released factors such as IL-4, IL-10, and TGFβ−1 (Milligan & Watkins, 2009). Interestingly, certain classes of transplanted cells (e.g., those derived from bone marrow) can alter microglia/macrophage recruitment after SCI (Busch et al., 2011; DePaul et al., 2015). We have also shown that astrocyte progenitors exhibit immunomodulatory properties in animal models of CNS disease, as they reduce microglial activation in cervical ventral horn in the $SOD1^{G93A}$ rat model of ALS (Lepore et al., 2008).

1.6 | Summary of current findings

An astrocyte lineage transplant that both can provide a cellular bridge for axon extension and that can contribute other beneficial properties such as modulating the pro-inflammatory macrophage response may be a powerful therapeutic tool capable of stimulating axon

growth and diaphragm recovery after cervical SCI. In the C2 hemisection model that involves disruption of rVRG axons, denervation of spared PhMNs located ipsilateral to the lesion and silencing of the hemi-diaphragm, we found that intraspinal transplantation of astrocyte progenitors promoted significant recovery of diaphragm function, stimulated robust regeneration of injured rVRG axons and sprouting of spared rVRG and serotonergic (5-HT) fibers, and reduced the macrophage response within the injured cervical spinal cord.

2 | MATERIALS AND METHODS

2.1 | Derivation and culturing of glial-restricted precursors

GRPs were isolated from the embryonic day-13.5 spinal cord of transgenic Fischer 344 rats that express human placental alkaline phosphatase (AP) under the ubiquitous Rosa 26 promoter, allowing for the in vivo tracking of transplant-derived cells as described previously (Lepore & Fischer, 2005). Cells were then plated onto 10 cm petri dishes coated with poly-D-lysine (13.3 μg/ml; Sigma-Aldrich, St. Louis, MO) in GRP basal medium (DMEM-F12, BSA [1 mg/ml; Sigma-Aldrich], B27 [Life Technologies, Grand Island, NY], bFGF [20 ng/ml; Peprotech; Rocky Hill, NJ], Pen-Strep [100 IU/ml; Life Technologies]; bFGF (10 μg/ml)] until transplantation.

2.2 | Preparation of GRPs for transplantation

Cultured GRPs were collected for transplantation at an in vitro time point no greater than three passages or 15 days postderivation (Han, Liu, Tyler-Polsz, Rao, & Fischer, 2004). On the day of transplantation, GRPs were trypsinized (Life Technologies) and centrifuged at 1500 rpm for 1 min; the supernatant was then discarded. The cell pellet was resuspended in 1 ml of GRP basal medium, and the cells were counted and then transferred into a 2 ml tube and centrifuged again at 300rcf for 3 min. The supernatant was removed and the cell pellet was kept on ice until transplantation. The final cell concentration was 200,000 cells/μl. Prior to conducting the large experiments presented in this study, we first tested various transplant conditions (i.e., number of injected cells and volume injected) to determine a paradigm for achieving robust transplant survival across the lesion site in this SCI model. We chose to only employ the injection paradigm that resulted in the most efficient engraftment in these pilot studies; nevertheless, we could test different transplantation conditions on diaphragm functional and axon regenerative efficacy in the future.

2.3 | Human dermal fibroblasts

Human dermal fibroblast cells were purchased from ATCC (Manassas, VA) and cultured with Fibroblast Growth Kit-grow serum (ATCC) (Li, Javed, Scura, et al., 2015b). They were prepared for transplantation as described in the previous section for GRPs.

2.4 | C2 hemisection and cell transplantation

Wild-type female Sprague–Dawley rats weighing 260–300 g were housed with ad libitum access to food and water. Experimental procedures were approved by the Thomas Jefferson University IACUC and conducted in compliance with ARRIVE (*Animal Research: Reporting of* in vivo *Experiments*) guidelines. Animals were separated into three groups: C2 hemisection + GRP transplantation ($n = 9$); C2 hemisection + fibroblast transplantation ($n =$

8); uninjured no-surgery ($n = 7$). Starting 4 days before transplantation and continuing until sacrifice, daily subcutaneous injections with 1 μl/g of 25% cyclosporine A (CSA) solution were administered for immunosuppression to all animals in all groups. On the day of surgery, animals were anesthetized via intraperitoneal injection of a cocktail of ketamine/acepromazine/xylazine. An incision was made in the cervical midline from the occipital bone to the midscapular line. The supraspinal muscles at this area were also incised and retracted to expose the vertebral column. A laminectomy was performed to expose the C2 spinal cord level. A micro-knife was used to make a paramedial incision in the dura mater.

After a right-sided hemisection was made, the lesion cavity was filled with 10 μl of either GRPs or fibroblasts using a gas-tight Hamilton syringe and a 33-gauge needle. To avoid washing out of cells from the lesion cavity, the dura mater was promptly closed using 9–0 sutures and then covered with Biobrane membrane and nucal fat before closure of the overlying muscle layers with 4–0 silk sutures and skin with surgical clips. Immediate postoperative care comprised of buprenorphine (with a reinforcement at 12 hr postoperative), 500 μl of Ringers' lactated serum (with additional doses given at 12 hr and 24 hr post-surgery) and 200 μl of cephazolin. The animals were kept overnight on a heating pad.

2.5 | rVRG axon tracing and quantification

Two weeks after injury, animals were anesthetized as described above for intra-brainstem injections of AAV2-mCherry. A midline incision was made at the base of the cranium using a sterile #11 blade. After deflection of the muscle and the C1/cranium ligament, the bone covering a portion of the brainstem was removed. Using a Hamilton Gas-tight Syringe (Hamilton, Reno, Nevada) with a 33-gauge needle, 0.3 μl of virus was injected 2 mm lateral (either right or left, depending on whether ipsilateral or contralateral rVRG tracing was being performed), 1 mm rostral and 2.6 mm ventral to the brainstem obex, using a stereotaxic apparatus (Kopf Instruments, Tujunga, CA) and an UltraMicroPump (World Precision Instruments, Sarasota, FL). The needle was left in place for 5 min before careful retrieval from the medulla. Postoperative care was given as described earlier. Spinal cord sections were analyzed for mCherry labeling using a Zeiss Imager M2 upright microscope with Metamorph Software. For ipsilaterally injected animals, areas of 100 μm in rostral-caudal length were outlined in sagittal spinal cord sections, starting at 800 μm rostral to the rostral intact-lesion border. Total numbers of rVRG-labeled fibers were counted in each of these 100 μm bins. For contralaterally injected animals, the numbers of individual rVRG-labeled axon profiles were counted specifically in the ventral horn of the C4 spinal cord ipsilateral to the lesion site (in a standard area size for every section).

2.6 | Electromyography and compound muscle action potentials recordings

At 35 days after injury and transplantation, animals were anesthetized using isoflurane. Compound muscle action potential (CMAP) recordings from the left and right hemidiaphragm were separately obtained, as previously described (Lepore et al., 2010). Briefly, a single stimulation (0.5 ms; 6 mV) of the phrenic nerve was performed by needle electrodes placed transcutaneously near the passage of the nerve in the neck. A ground electrode was placed in the tail, and reference electrode was inserted in the abdominal

region. A surface strip electrode was placed along the costal margin of the hemi-diaphragm. CMAP recordings were obtained using an ADI Powerlab 8/30 stimulator and BioAMP amplifier (ADInstruments, Colorado Springs, CO), followed by computer-assisted data analysis (Scope 3.5.6, ADInstruments). For each animal, 10–20 tracings were averaged. Following CMAP recording, a right upper quadrant laparotomy was performed to expose the inferior surface of the hemi-diaphragm. Bipolar electrodes spaced 3 mm apart were introduced to obtain electromyography (EMG) recordings from the three diaphragmatic subregions (for at least 2 min each) during normal eupnic breathing (Li, Javed, Scura, et al., 2015b). The EMG signal was amplified, filtered through a band-pass filter (50–3,000 Hz) and integrated using LabChart 7 software (ADInstruments).

2.7 | Perfusion, tissue harvesting and sectioning

Immediately following EMG recordings, animals were injected with 0.22 mg/g Euthasol, transcardially perfused, and dissection of the CNS and diaphragm was performed. A 1 cm rostral-to-caudal length of the cervical spinal cord was embedded in tissue freezing medium (TFM; (General Data, Cincinnati, OH). Sagittal or transverse 30 μm sections were cut using a cryostat (Thermo Scientific, Philadelphia, PA) and mounted on Fisher tissue frost slides (Fisher Scientific, Pittsburgh, PA).

2.8 | Immunohistochemistry

Slides were taken from the 4°C refrigerator and allowed to dry at room temperature for at least 1 hr. The slides were then washed 3× for 5 min with 1× PBS before 1 hr of incubation with blocking buffer (5% normal horse serum [Vector Laboratories, Burlingame, CA], 0.2% triton X-100 [Amresco, Solon, OH] in PBS). After blocking, the primary antibody or antibodies diluted in blocking solution were added to the slides and incubated overnight at 4°C. The complete list of antibodies used and their dilutions are described in Table 1. On the following day, slides were washed 3× for 5 min with PBS before incubation with secondary antibody (diluted 1:200 in blocking solution) for 1 hr at room temperature in the dark. Slides were then washed again 3× for 10 min in PBS, and Fluorsave solution (Calbiochem, San Diego, CA) was added before cover slipping. Imaging was performed using a Zeiss Imager M2 upright microscope with Metamorph Software and analyzed using ImageJ software.

2.9 | Immunocytochemistry

GRPs and fibroblasts were plated on 2 cm diameter cover slips coated with poly-d-lysine in 24-well plates. After 2 days, the cells were washed 2 times with PBS and then fixed using 4% paraformaldehyde for 10 min. Three more washes with PBS for 5 min each were performed before proceeding to immunostaining (as described above for immunohistochemistry on spinal cord tissue sections). Cover slips were then collected from the wells and flipped over onto a glass slide using Fluorosave reagent.

2.10 | Lesion size analysis

Sagittal sections of cervical spinal cord were immunostained with NeuN antibody, as described earlier (Lepore et al., 2011). Images taken with a Zeiss Imager M2 upright microscope, and using Metamorph software the rostral-to-caudal distance between lesion-

spared tissue interfaces (i.e., on the rostral and caudal sides of the lesion) were measured at three different dorsal–ventral locations and averaged (Falnikar, Hala, Poulsen, & Lepore, 2016). This analysis was always performed at the same medial-lateral position of the right hemi-cord.

2.11 | Neuromuscular junction morphology analysis

Fresh hemi-diaphragm muscle was dissected from each animal for whole-mount immunohistochemistry, as described previously (Nicaise, Hala, Frank, et al., 2012a). The muscle was dissected, stretched, pinned down to Sylgard medium (Fisher Scientific) and cleaned. Motor axons and their terminals were labeled with SMI-312R (Covance, Princeton, NJ; 1:1000) and SV2-s (DSHB, Iowa City, IA; 1:10), respectively. Detection of these antibodies was made with FITC anti-mouse IgG secondary (Jackson ImmunoResearch Laboratories, West Grove, PA; 1:100). Postsynaptic acetylcholine receptors were labeled with rhodamine-conjugated alpha-bungarotoxin (Life Technologies; 1:400). Labeled muscles were imaged using a FluoView FV1000 confocal microscope (Olympus, Center Valley, PA) and analyzed for total numbers of NMJs and intact and denervated NMJs.

2.12 | 5-HT axon analysis

Three sagittal spinal cord sections from each animal were immunostained with 5-HT antibody, as previously described (Ohtake et al., 2014). Numbers of 5-HT-labeled axon profiles were counted with Metamorph software specifically within the ipsilateral ventral horn at three distances caudal to the lesion (1,500, 3,000, and 4,500 μm) on images taken with a Zeiss Imager M2 upright microscope.

2.13 | Macrophage analysis

For time-course analysis of macrophage labeling after hemisection SCI, animals were injured as described earlier. Animals were then sacrificed at 1, 10, or 35 days postinjury. IHC was performed as described above using ED1 (CD68) primary antibody at a concentration of 1:300. Images of ED1 immunostaining were taken using a Zeiss Imager M2 upright microscope with Metamorph software. Total numbers of ED1 + cells were counted in a standardized area size within the lesion site in three separate sections per animal (and averaged) using ImageJ software. The same method was used to count the number of ED1+ cells and the ED1 fluorescence intensity within the lesion of GRP- and fibroblast-transplanted animals. We also quantified numbers of ED1+ cells within the ventral horn ipsilateral to the hemisection at 0, 1,500, 3,000, and 4,000 μm caudal to the caudal lesion–intact spinal cord interface.

2.14 | Statistics

Values were expressed as mean ± standard deviation. For all analyses, three separate sections or three separate wells/dishes per sample were analyzed and averaged. Statistical significance was considered for p-values of <.05. All statistical analysis was performed using GraphPad Prism version 6.01 for Windows (GraphPad Software, La Jolla CA).

3 | RESULTS

3.1 | GRPs differentiated into astrocytes in vitro

To achieve targeted delivery of astrocytes to the injured spinal cord using a transplantation-based approach, we used glial-restricted precursors (GRPs) derived from the developing rat spinal cord. We isolated GRPs from the embryonic day-13.5 spinal cord of transgenic rats expressing the human placental alkaline phosphatase (AP) gene in all cells of the body; transplantation of AP-labeled cells allowed for the differential identification of transplant-derived cells in the spinal cord of wild-type animals (Lepore et al., 2008; Lepore & Fischer, 2005). Undifferentiated AP+ GRPs maintained a glial progenitor-like morphology in culture (Figure 1a). When stimulated to differentiate into astrocytes by mitogen removal and the addition of BMP-4, GRPs acquired an astrocyte-like morphology in vitro (Figure 1b). Prior to astrocyte differentiation, nearly all cells in the GRP culture expressed the immature neural stem/progenitor cell marker nestin (Figure 1c) but did not express the astrocyte marker GFAP (Figure 1e), while differentiated GRP-derived astrocytes did not express nestin (Figure 1d) but highly expressed GFAP (Figure 1F). Although GRPs are bipotential glial progenitors that can generate both astrocytes and oligodendrocytes (Rao & Mayer-Proschel, 1997; Rao, Noble, & Mayer-Proschel, 1998), a targeted differentiation protocol resulted in efficient differentiation of nearly all GRPs into GFAP-expressing astrocytes in vitro (Figure 1g). As a nonglial cell transplant control, we used dermal fibroblasts (Li, Javed, Scura, et al., 2015b), which can be expanded in culture prior to transplantation (Figure 1h).

3.2 | GRP transplants survived long-term and efficiently differentiated into astrocytes in the injured cervical spinal cord

We next determined the in vivo fate of GRP transplants following intraspinal injection directly into the lesion site immediately after C2 hemisection. AP-labeled GRP-derived cells robustly survived within the lesion for at least 5 weeks post-transplantation (Figure 2a), which was the latest time point assessed in this study (although we have previously shown survival of GRP transplants up to at least 18 months postinjection [Lepore et al., 2006]). Similarly, fibroblasts survived well in the lesion site until the 5-week point of sacrifice, as assessed by the human-specific marker HuNA (Figure 2b). We also have examined the presence of AP+ transplant-derived cells at distances from the lesion implantation site. We found no AP-labeled cells at 1 cm rostral or 1 cm caudal to the lesion site within the spinal cord or in the medulla at levels close to the rVRG (data not shown). Given the potential for persistent uncontrolled proliferation of transplants derived from stem and progenitor cells, we examined continued cell division of GRP transplants. At 5 weeks postinjection, AP+ cells did not continue to express the proliferation marker Ki67 (Figure 2c). To assess the differentiation of transplant-derived cells in vivo, we double labeled for AP and markers of astrocytes (GFAP), neurons (NeuN), and cells of the oligodendrocyte lineage (Olig2). The vast majority of AP+ cells (93.65% ± 5.56%) at 5 weeks post-transplantation differentiated into GFAP+ astrocytes (Figure 2d), while no GRPs differentiated into NeuN+ neurons (0.0 ± 0.0%) or Iba1+ microglia/macrophages (0.0 ± 0.0%) and few generated APC+ oligodendrocytes (0.0 ± 0.0% in the lesion).

3.3 | GRP transplantation promoted significant recovery of diaphragm electromyography amplitudes

To assess diaphragmatic respiratory function in vivo, we conducted EMG recordings from the hemidiaphragm ipsilateral to the hemisection in anesthetized animals (Nicaise, Hala, Frank, et al., 2012a; Nicaise, Putatunda, Hala, et al., 2012b; Nicaise et al., 2013). We performed these EMG recordings from three different subregions of the hemidiaphragm as these subregions are innervated by PhMNs located at different locations within the C3–5 spinal cord (Laskowski & Sanes, 1987). In general, the dorsal part of the hemidiaphragm is primarily innervated by PhMNs whose cell bodies are located at C5, the medial diaphragm is innervated by C4 PhMNs, and the ventral subregion is innervated by PhMNs found in the C3 spinal cord. We measured inspiratory EMG bursts during normal eupnic breathing. Compared with uninjured control (Figure 3a), C2 hemisection animals receiving either fibroblast (Figure 3b) or GRP (Figure 3c) transplantation showed reduced inspiratory bursts. In the case of fibroblast-injected rats, the hemidiaphragm was almost completely silent at 5 weeks post-SCI, which was similar to rats that receive C2 hemisection alone (data not shown) (Alilain, Horn, Hu, Dick, & Silver, 2011). At all three subregions of the hemi-diaphragm, GRPs significantly increased EMG burst amplitudes compared with fibroblast control transplants (Figure 3c,g), demonstrating substantial recovery of diaphragm function. In the dorsal region, GRP-induced recovery was only partial, as there was still a significant difference between the GRP and uninjured/laminectomy-only groups. In the medial and ventral subregions, EMG amplitudes in the GRP group were not statistically different than uninjured controls, suggesting that the GRPs exerted greater effects on PhMNs located at more rostral locations within the cervical spinal cord. As the means were substantially lower for the GRP animals than the laminectomy-only rats at medial and ventral subregions (even if these differences were not statistically significant), a claim of complete recovery cannot be made.

3.4 | GRPs did not affect lesion size in the cervical spinal cord or functional and morphological innervation at the diaphragm neuromuscular junction

We previously reported that GRP transplants reduced PhMN degeneration and lesion size following injection into the C4 contusion SCI model (Li, Javed, Hala, et al., 2015a). To determine whether GRPs exerted similar neuroprotective effects on PhMN-diaphragm circuitry in the current study, we quantified lesion size and both functional and morphological innervation of the diaphragm at 5 weeks post-SCI. To assess functional innervation of the ipsilateral hemidiaphragm, we conducted CMAP recordings in response to supramaximal stimulation of the phrenic nerve in anesthetized rats (Li et al., 2014). Compared with uninjured controls (Figure 3d), we did not observe a reduction in CMAP amplitudes in C2 hemisection animals receiving either fibroblast (Figure 3e) or GRP (Figure 3f) injections. Furthermore, there was no difference in CMAP amplitudes between fibroblast and GRP groups (Figure 3h). To assess morphological innervation of the neuromuscular junction (NMJ) in ipsilateral hemidiaphragm, we performed detailed confocal analysis of individual NMJs across the muscle (Lepore et al., 2010). We labeled phrenic motor axons all the way to their presynaptic terminals with SMI-312 and SV-2 (Figure 4a), and we labeled postsynaptic nicotinic acetylcholine receptors in the muscle with Alexa-conjugated α-bungarotoxin (Figure 4b). Nearly 100% of NMJs at all three subregions of the

hemidiaphragm were completely intact (Figure 4a–c), and there were no differences in the percentage of innervated and denervated NMJs between fibroblasts and GRPs at any subregion (Figure 4d). As the C2 hemisection was located rostral to the PhMN pool, the absence of PhMN loss and diaphragm denervation is not unexpected; nevertheless, we conducted these analyses to rule out possible effects of GRPs directly on PhMNs. We also quantified lesion size by measuring the rostral-to-caudal length of the lesion in sagittal sections and found no difference between fibroblast and GRP animals (Figure 4e).

3.5 | GRPs stimulated robust regeneration of injured rVRG axons but no synaptic reconnection of these regrowing fibers with PhMNs

We next examined the effects of GRP transplantation on axonal growth. We first labeled all axon populations with the pan-neuronal neurofilament marker SMI-312 at 5 weeks post-SCI. GRPs stimulated significant ingrowth of SMI-312+ axons into the lesion (Figure 5a). On the contrary, in the control animals that received fibroblast transplantation, a high density of SM1–312+ axons were located in the intact spinal cord directly adjacent to the lesion site; however, we observed almost no growth of SM1–312+ axons across the lesion–intact interface (Figure 5b). Compared with fibroblasts, GRPs significantly increased both the number of SMI-312+ axons profiles (Figure 5c) and the density of these axons (Figure 5d) within the lesion site. Confocal imaging shows that most of these SMI-312+ fibers in the lesion extended along AP +/GFAP+ cells (Figure 5e), demonstrating that axons regenerated along transplant-derived astrocytes within the lesion site. To specifically label rVRG axons, we stereotaxically injected the anterograde axonal tracer AAV2-mCherry into the ipsilateral rVRG 2 weeks prior to sacrificing animals at 5 weeks post-SCI (Figure 6a,b). We have previously shown that with this labeling approach we can selectively transduce only neurons of the rVRG. GRPs stimulated robust regeneration of mCherry+ rVRG axons across the rostral intact–lesion border (Figure 6d–d”). On the contrary, in the control fibroblast animals, all mCherry-labeled rVRG axons stop at the border between the rostral intact spinal cord and the lesion, with many of these axons retracting back from the injury site (Figure 6e). No rVRG axons regenerate into the lesion site with fibroblast transplantation. We quantified numbers of mCherry+ axon profiles in sagittal sections at defined rostral-caudal distances relative to the rostral end of the lesion (Figure 6f). We find that GRPs reduced retraction of rVRG axons in the rostral intact spinal and stimulated significant regeneration across the entire lesion site. We selectively labeled ipsilateral PhMNs by intrapleurally injecting the retrograde tracer cholera toxin B (Li et al., 2014). This labeling shows that the PhMN pool is located directly caudal to the hemisection (Figure 6C); however, regenerating rVRG fibers did not reinnervate these PhMNs as no rVRG axons crossed the caudal lesion–intact interface to re-enter distal spinal cord (Figure 6f).

3.6 | GRPs induced substantial sprouting of spared axons originating in contralateral rVRG

Although substantial, the regeneration of injured ipsilateral rVRG axons induced by GRP transplantation was likely not responsible for driving functional diaphragm recovery. While restoration of the original pre-injury rVRG-PhMN circuitry (i.e., monosynaptic input to PhMNs from ipsilateral rVRG) is a major goal for improving respiratory function after cervical SCI, additional circuit plasticity mechanisms may also be able to promote recovery.

Most human SCI cases are anatomically incomplete (Ahuja et al., 2017), providing a substrate of spared axons that can sprout to form novel connections for reinnervating neuronal populations distal to a spinal cord lesion. In the C2 hemisection paradigm, the descending axons originating in the contralateral rVRG are intact and, even both in the uninjured spinal cord (data not shown) and in the control C2 hemisection condition (Figure 7b–d), there is some projection of these rVRG fibers into the PhMN pool ipsilateral to the injury site. To determine the effects of GRP transplantation on the growth response of these axons, we injected AAV2-mCherry into the contralateral rVRG in a separate cohort of C2 hemisection animals receiving fibroblast or GRP transplantation (Figure 7a). We quantified the sprouting of these mCherry-labeled rVRG axons specifically within the C4 ventral horn ipsilateral to the hemisection (i.e., the location of PhMN soma) (Figure 7e) at 5 weeks post-SCI. Interestingly, in C2 hemisection rats, GRPs promoted significant sprouting of contralateral rVRG axons within the ipsilateral ventral horn at level C4 compared with fibroblast control (Figure 7f–h).

3.7 | GRPs enhanced 5-HT axon growth within the PhMN pool

In addition to rhythmic excitatory drive to PhMNs from the rVRG, PhMN excitability is also modulated by descending 5-HT input (Warren et al., 2014). Similar to our analysis of contralateral rVRG sprouting, we assessed 5-HT axonal input to the PhMN pool specifically in the ventral horn ipsilateral/caudal to the lesion (Figure 7c). We performed 5-HT immunohistochemistry at 5 weeks post-SCI and quantified the numbers of 5-HT axonal profiles within the ipsilateral ventral horn at spinal cord level containing the PhMN pool (Figure 8a). Compared with fibroblasts, GRP-transplanted animals showed significantly greater numbers of 5-HT axon profiles throughout the PhMN pool at levels C3, C4, and C5 (Figure 8b).

3.8 | GRPs significantly reduced the macrophage response both within the lesion site and in the intact caudal spinal cord surrounding PhMNs

Given the immunomodulatory properties of astrocytes (Sofroniew, 2015) and the role played by macrophages in inducing axonal die-back and limiting regrowth (Silver et al., 2015), we examined whether GRP transplantation altered the macrophage response both within the lesion site and at intact caudal locations where PhMNs reside. We first characterized the temporal progression of the macrophage response within the C2 hemisection site using the marker ED1, which labels both infiltrating peripheral monocyte-derived macrophages and resident microglial-derived macrophages. There were almost no ED1+ cells in the intact spinal cord at C2 in laminectomy-only control rats (Figure 9a). There was a substantial increase in ED1+ cell counts by 1 day postinjury (Figure 9b), and these counts progressively increased out to 10 days (Figure 9c) and 35 days (Figure 9d) post-SCI (Figure 9e), demonstrating a robust and persistent macrophage response that may be involved in limiting rVRG and 5-HT axon growth following cervical SCI. We next quantified the ED1 response following transplantation at 5 weeks post-SCI. Compared with fibroblasts (Figure 9f), GRPs significantly reduced the number of ED1+ cells (Figure 9g,h) and the intensity of ED1 immunostaining (Figure 9g,i) in the lesion site. Because we observed substantial rVRG and 5-HT axon sprouting around ipsilateral PhMNs, we also quantified the macrophage response caudal to the lesion. Hemisection SCI induced a pronounced macrophage response even at

these intact locations removed from the lesion (Figure 9j–k). Compared with fibroblasts (Figure 9j–j”), GRPs reduced the numbers of ED1+ cells in the ipsilateral C3–C5 ventral horn (Figure 9k–k”) at 5 weeks post-hemisection (Figure 9l). Collectively, these ED1 data suggest that the immunomodulatory effects of GRP transplantation on the macrophage response both within the lesion and at distal locations may possibly have mediated the GRP effects on rVRG axon regeneration and sprouting of spared rVRG and 5-HT fibers.

4 | DISCUSSION

4.1 | Summary of findings

Our results show that intraspinal transplantation of astrocyte progenitors in the C2 hemisection model of SCI promoted: (a) significant recovery of diaphragmatic respiratory function, (b) robust regeneration of damaged bulbospinal rVRG axons, (c) extensive sprouting of both spared contralateral rVRG axons and 5-HT fibers, and (d) a pronounced reduction in the axonal growth-inhibitory macrophage response both in the lesion site and surrounding PhMNs in the intact spinal cord distal to the lesion. We evaluated several neuroanatomical mechanisms of axon growth and rVRG-PhMN-diaphragm circuit connectivity that may underlie the significant diaphragm recovery we observed in response to GRP transplantation. Specifically, we explored (a) regeneration of injured ipsilateral rVRG axons, (b) sprouting of spared contralateral rVRG pathways, and (c) growth of descending serotonergic axons that modulate excitatory drive to PhMNs.

4.2 | Astrocyte progenitor transplantation promoted regeneration of bulbospinal respiratory axons

We showed that GRP transplantation induced regeneration of injured ipsilateral rVRG axons into and across the lesion site; however, these axons did not re-enter intact spinal cord distal to the hemisection site. It is possible that these axons did not exit the lesion/graft site because the transplants were especially hospitable to the extending fibers, while the lesion–intact interface provided formidable barriers such as environmental growth inhibitors (Bradbury et al., 2002; Giger et al., 2010). In addition, because nearly all transplant-derived cells remained localized to the lesion site, the beneficial effects of GRPs on the macrophage response was most pronounced within the lesion; therefore, regenerating rVRG axons may not have exited the lesion site because of increased macrophage infiltration immediately distal to the hemisection. In fact, we observed the most robust reduction of macrophage infiltration within the lesion at locations where GRP-derived astrocytes were located (compared with other areas within the lesion that were devoid of transplanted cells) (data not shown). Despite this extensive axon regeneration, we believe that this mechanism did not drive functional recovery as these regrowing fibers did not reconnect with PhMNs located caudal to the injury.

4.3 | GRP transplants also stimulated sprouting of spared axon populations that control diaphragm function

We also demonstrated that GRPs stimulated extensive sprouting of spared contralateral rVRG axons and 5-HT axons within the ventral horn ipsilateral/caudal to the hemisection, suggesting that the generation of alternative circuits may be responsible for functional

improvement. We and others have observed a small degree of spontaneous recovery of EMG bursting in the ipsilateral hemi-diaphragm after C2 hemisection, and a number of studies have shown that this recovery is mediated by pathways descending in the contralateral hemi-cord (Dale-Nagle et al., 2010). Therefore, it is possible that GRP transplantation greatly enhanced a plasticity response that occurs to a small degree after high-cervical SCI even without therapeutic intervention. While long-distance regeneration of injured axons is an important target for circuit restoration and functional improvement after SCI, local sprouting of spared fibers is a promising form of plasticity that may be a more easily attainable goal. In these studies, we did not determine whether sprouting rVRG and/or 5-HT axons made mono-synaptic connections with PhMNs or whether the GRP-induced circuit was polysynaptic involving, for example, pre-phrenic interneurons (Lane et al., 2008b); we are exploring this important issue in ongoing studies.

The vast majority of transplant-derived astrocytes were located within the lesion, raising the question of how GRPs stimulated sprouting in the intact caudal spinal cord, including up to three spinal cord segments away at C5. Using secretome analysis on cultured GRPs, we have found that both GRPs and GRP-derived astrocytes release a host of immunomodulatory factors, including a number of anti-inflammatory molecules (Goulão et al., unpublished findings). This suggests that the GRP transplants may have stimulated axon sprouting throughout the PhMN pool by releasing factors over a relatively long distance to dampen the macrophage response that limits axonal growth after SCI.

4.4 | GRPs did not exert neuroprotective effects

We previously demonstrated significant neuroprotective properties of astrocyte progenitor transplants (Li, Javed, Hala, et al., 2015a; Li, Javed, Scura, et al., 2015b). However, we conducted these studies with acute injection into a contusion SCI paradigm that involves pronounced secondary degeneration, while this C2 hemisection model does not exhibit much secondary expansion of the lesion. In the current study, we observed no effects of GRPs on lesion size. In addition, we found no effects on PhMN innervation of the ipsilateral hemi-diaphragm using both CMAP recordings to assess functional innervation and NMJ analysis to test morphological innervation. These results further support the notion that recovery induced by GRPs was likely due to central changes within the spinal cord involving plasticity in descending axonal input to PhMNs (rVRG, 5-HT or both).

In the present work, we only tested transplantation at the time of hemisection as a proof-of-principle. Given the clinical relevance of delayed intervention following SCI, in ongoing work, we are currently evaluating the effects of GRP delivery on diaphragm function, rVRG and 5-HT axonal plasticity and the intraspinal inflammatory response.

4.5 | Astrocyte lineage transplantation is a novel approach for targeting respiratory dysfunction following SCI

Despite the profound importance of treating respiratory dysfunction in SCI, relatively few studies have been conducted to promote targeted reconnection of the circuitry that controls critical respiratory muscles such as the diaphragm, particularly using cell transplantation-based approaches (Charsar, Urban, & Lepore, 2017). We evaluated the therapeutic potential

of transplantation-based delivery of astrocytes via an approach that has not been extensively explored to date in the context of targeting respiratory dysfunction (Nakamura & Okano, 2013). Using intraspinal transplantation of rodent GRPs or human-induced pluripotent stem cell-derived astrocytes, we previously showed that astrocyte line-age transplants can preserve diaphragm function in the mid-cervical contusion SCI model by restoring astrocyte glutamate transporter expression and extracellular glutamate homeostasis and consequently reducing excitotoxic degeneration of PhMNs (Li, Javed, Hala, et al., 2015a; Li, Javed, Scura, et al., 2015b). In this study, we have demonstrated that similar transplants also promote substantial axonal growth and can modulate the inflammatory response following cervical SCI. A body of previous work has also shown that transplantation of astrocyte progenitors or differentiated astrocytes promote axon growth in animal models of CNS trauma, including SCI (Davies et al., 2006; Davies et al., 2008; Haas et al., 2012; Haas & Fischer, 2013; Shih, Lacagnina, Leuer-Bisciotti, & Proschel, 2014; Smith, Miller, & Silver, 1986; Smith, Miller, & Silver, 1987; Smith, Rutishauser, Silver, & Miller, 1990; Smith & Silver, 1988); however, these studies did not address respiratory compromise or immunomodulation. Collectively, our work and the findings of others demonstrate that astrocyte lineage transplantation can provide therapeutic benefit for SCI via a number of important cellular mechanisms, which is not surprising given the critical role played by astrocytes in a host of CNS functions during development, in the intact adult brain and spinal cord, and in the context of nervous system pathology (Pekny & Nilsson, 2005).

4.6 | Astrocyte progenitor transplantation modulated the intraspinal macrophage response

We took a novel approach by examining the immunomodulatory capacity of astrocyte lineage transplantation after SCI. We used the pan-macrophage marker ED1 to quantify the macrophage response at various anatomical locations relevant to restoration of diaphragm function. However, the effect of macrophages on axon growth is likely not as simple as a dichotomy of “resting” versus “activated” microglia/macrophages. Instead, it appears that (a) spinal cord microglia/macrophages exist along a continuum of phenotypes, (b) that these various sub-populations simultaneously exist within the diseased nervous system, and (c) their makeup is constantly changing over time postinsult (Hu et al., 2015). One way to view this complexity (which is subject to debate [Ransohoff, 2016]) is that macrophages exist along this spectrum in either an M1-like pro-inflammatory or M2-like tissue reparative phenotype (Hu et al., 2015). Macrophages transition along the M1-to-M2 spectrum during normal wound-healing throughout the body. However, this process appears to be compromised in SCI, with a bias toward a persistent M1 response that does not result in successful tissue repair (Gensel & Zhang, 2015). Importantly, this M1 state is involved in outcomes such as axonal die-back near the SCI lesion site (Silver et al., 2015) and abnormal pain transmission after nervous system injury (Ristoiu, 2013), in part due to the release of factors such as pro-inflammatory cytokines (e.g., IL-1B, TNF-alpha and IL-6) (Mika, Zychowska, Popiolek-Barczyk, Rojewska, & Przewlocka, 2013). In future work, it will be important to determine whether GRP transplants can (in addition to altering the overall macrophage response, as revealed by our ED1 analysis) bias this response away from a M1 pro-inflammatory phenotype and toward a M2-like tissue reparative phenotype, which may provide an environment in and around the lesion that is conducive to axon growth. As we

only conducted analysis of axonal growth and macrophage response following GRP injection at a single late time point post-injury, it will also be important in future work to perform these analyses at multiple intermediate times to better understand the impact of immunomodulation on the rVRG and 5-HT axonal growth both in the lesion and at the intact caudal locations.

Although we focused on the immunomodulatory influence of transplants in this study, GRPs may be able to affect axonal plasticity via additional processes such as through the release of trophic factors. We previously quantified intraspinal levels of BDNF, IGF-1 and VEGF using ELISA following transplantation of GRPs into the cervical spinal cord of the SOD1^{G93A} rat model of ALS (Lepore et al., 2008) We found that GRP transplantation did not affect levels of any of these molecules within the spinal cord, suggesting that GRPs are likely not stimulating rVRG and 5-HT axonal growth by a trophic factor-mediated mechanism in the current work.

5 | CONCLUSIONS

Our findings suggest that transplantation-based delivery of astrocytes to the injured spinal cord is a promising approach for promoting respiratory recovery, a critical goal for the treatment of individuals affected by SCI. Our data also shed light on novel mechanisms by which astrocyte progenitor transplants can promote plasticity in injured and spared neural circuits following SCI; these results are relevant to diaphragm function but also to the host of other circuits and functional outcomes disrupted by spinal cord trauma.

ACKNOWLEDGMENTS

This work was funded by the NINDS (2R01NS079702–06 to A.C.L.) and the Paralyzed Veterans of America Research Foundation (Grant 476686 to A.C.L).

Funding information

National Institute of Neurological Disorders and Stroke, Grant/Award Number: 2R01NS079702–06 (to A.C.L.); Paralyzed Veterans of America Research Foundation, Grant/Award Numbers: Grant 476686 (to A.C.L), 476686; NINDS, Grant/Award Number: R01NS079702–06

REFERENCES

Ahuja CS, Wilson JR, Nori S, Kotter MRN, Druschel C, Curt A, & Fehlings MG (2017). Traumatic spinal cord injury. Nature Reviews Disease Primers, 3, 17018.

Alilain WJ, Horn KP, Hu H, Dick TE, & Silver J (2011). Functional regeneration of respiratory pathways after spinal cord injury. Nature, 475, 196–200. [PubMed: 21753849]

Bradbury EJ, Moon LD, Popat RJ, King VR, Bennett GS, Patel PN, … McMahon SB (2002). Chondroitinase ABC promotes functional recovery after spinal cord injury. Nature, 416, 636–640. [PubMed: 11948352]

Busch SA, Hamilton JA, Horn KP, Cuascut FX, Cutrone R, Lehman N, … Silver J (2011). Multipotent adult progenitor cells prevent macrophage-mediated axonal dieback and promote regrowth after spinal cord injury. The Journal of Neuroscience, 31, 944–953. [PubMed: 21248119]

Calvo M, & Bennett DL (2012). The mechanisms of microgliosis and pain following peripheral nerve injury. Experimental Neurology, 234, 271–282. [PubMed: 21893056]

Charsar BA, Urban MW, & Lepore AC (2017). Harnessing the power of cell transplantation to target respiratory dysfunction following spinal cord injury. Experimental Neurology, 287, 268–275. [PubMed: 27531634]

Clark AK, Old EA, & Malcangio M (2013). Neuropathic pain and cytokines: Current perspectives. Journal of Pain Research, 6, 803–814. [PubMed: 24294006]

Dale-Nagle EA, Hoffman MS, MacFarlane PM, Satriotomo I, Lovett-Barr MR, Vinit S, & Mitchell GS (2010). Spinal plasticity following intermittent hypoxia: Implications for spinal injury. Annals of the New York Academy of Sciences, 1198, 252–259. [PubMed: 20536940]

Davies JE, Huang C, Proschel C, Noble M, Mayer-Proschel M, & Davies SJ (2006). Astrocytes derived from glial-restricted precursors promote spinal cord repair. Journal of Biology, 5, 7. [PubMed: 16643674]

Davies JE, Proschel C, Zhang N, Noble M, Mayer-Proschel M, & Davies SJ (2008). Transplanted astrocytes derived from BMP- or CNTF-treated glial-restricted precursors have opposite effects on recovery and allodynia after spinal cord injury. Journal of Biology, 7, 24. [PubMed: 18803859]

DePaul MA, Palmer M, Lang BT, Cutrone R, Tran AP, Madalena KM, … Silver J (2015). Intravenous multipotent adult progenitor cell treatment decreases inflammation leading to functional recovery following spinal cord injury. Scientific Reports, 5, 16795. [PubMed: 26582249]

Falnikar A, Hala TJ, Poulsen DJ, & Lepore AC (2016). GLT1 overexpression reverses established neuropathic pain-related behavior and attenuates chronic dorsal horn neuron activation following cervical spinal cord injury. Glia, 64, 396–406. [PubMed: 26496514]

Falnikar A, Li K, & Lepore AC (2015). Therapeutically targeting astrocytes with stem and progenitor cell transplantation following traumatic spinal cord injury. Brain Research, 1619, 91–103. [PubMed: 25251595]

Gensel JC, & Zhang B (2015). Macrophage activation and its role in repair and pathology after spinal cord injury. Brain Research, 1619, 1–11. [PubMed: 25578260]

Giger RJ, Hollis ER, 2nd, & Tuszynski MH (2010). Guidance molecules in axon regeneration. Cold Spring Harbor Perspectives in Biology, 2, a001867. [PubMed: 20519341]

Graeber MB, & Christie MJ (2012). Multiple mechanisms of microglia: A gatekeeper's contribution to pain states. Experimental Neurology, 234, 255–261. [PubMed: 22273537]

Haas C, & Fischer I (2013). Human astrocytes derived from glial restricted progenitors support regeneration of the injured spinal cord. Journal of Neurotrauma, 30, 1035–1052. [PubMed: 23635322]

Haas C, Neuhuber B, Yamagami T, Rao M, & Fischer I (2012). Phenotypic analysis of astrocytes derived from glial restricted precursors and their impact on axon regeneration. Experimental Neurology, 233, 717–732. [PubMed: 22101004]

Hamby ME, & Sofroniew MV (2010). Reactive astrocytes as therapeutic targets for CNS disorders. Neurotherapeutics: the journal of the American Society for Experimental NeuroTherapeutics, 7, 494–506. [PubMed: 20880511]

Han SS, Liu Y, Tyler-Polsz C, Rao MS, & Fischer I (2004). Transplantation of glial-restricted precursor cells into the adult spinal cord: Survival, glial-specific differentiation, and preferential migration in white matter. Glia, 45, 1–16. [PubMed: 14648541]

Harvey AR, Lovett SJ, Majda BT, Yoon JH, Wheeler LP, & Hodgetts SI (2015). Neurotrophic factors for spinal cord repair: Which, where, how and when to apply, and for what period of time? Brain Research, 1619, 36–71. [PubMed: 25451132]

Hill CE, Proschel C, Noble M, Mayer-Proschel M, Gensel JC, Beattie MS, & Bresnahan JC (2004). Acute transplantation of glialrestricted precursor cells into spinal cord contusion injuries: Survival, differentiation, and effects on lesion environment and axonal regeneration. Experimental Neurology, 190, 289–310. [PubMed: 15530870]

Hu X, Leak RK, Shi Y, Suenaga J, Gao Y, Zheng P, & Chen J (2015). Microglial and macrophage polarization-new prospects for brain repair. Nature Reviews Neurology, 11, 56–64. [PubMed: 25385337]

Lane MA, Fuller DD, White TE, & Reier PJ (2008a). Respiratory neuroplasticity and cervical spinal cord injury: Translational perspectives. Trends in Neurosciences, 31, 538–547. [PubMed: 18775573]

Lane MA, Lee KZ, Fuller DD, & Reier PJ (2009). Spinal circuitry and respiratory recovery following spinal cord injury. Respiratory Physiology & Neurobiology, 169, 123–132.

Lane MA, White TE, Coutts MA, Jones AL, Sandhu MS, Bloom DC, … Reier PJ (2008b). Cervical prephrenic interneurons in the normal and lesioned spinal cord of the adult rat. The Journal of Comparative Neurology, 511, 692–709. [PubMed: 18924146]

Laskowski MB, & Sanes JR (1987). Topographic mapping of motor pools onto skeletal muscles. The Journal of Neuroscience, 7, 252–260. [PubMed: 3543250]

Lepore AC, & Fischer I (2005). Lineage-restricted neural precursors survive, migrate, and differentiate following transplantation into the injured adult spinal cord. Experimental Neurology, 194, 230–242. [PubMed: 15899260]

Lepore AC, Neuhuber B, Connors TM, Han SS, Liu Y, Daniels MP, … Fischer I (2006). Long-term fate of neural precursor cells following transplantation into developing and adult CNS. Neuroscience, 139, 513–530. [PubMed: 16458439]

Lepore AC, O'Donnell J, Kim AS, Yang EJ, Tuteja A, Haidet-Phillips A, … Maragakis NJ (2011). Reduction in expression of the astrocyte glutamate transporter, GLT1, worsens functional and histological outcomes following traumatic spinal cord injury. Glia, 59, 1996–2005. [PubMed: 21882244]

Lepore AC, Rauck B, Dejea C, Pardo AC, Rao MS, Rothstein JD, & Maragakis NJ (2008). Focal transplantation-based astrocyte replacement is neuroprotective in a model of motor neuron disease. Nature Neuroscience, 11, 1294–1301. [PubMed: 18931666]

Lepore AC, Tolmie C, O'Donnell J, Wright MC, Dejea C, Rauck B, … Maragakis NJ (2010). Peripheral hyperstimulation alters site of disease onset and course in SOD1 rats. Neurobiology of Disease, 39, 252–264. [PubMed: 20381620]

Li K, Javed E, Hala TJ, Sannie D, Regan KA, Maragakis NJ, … Lepore AC (2015a). Transplantation of glial progenitors that overex-press glutamate transporter GLT1 preserves diaphragm function following cervical SCI. Molecular Therapy, 23, 533–548. [PubMed: 25492561]

Li K, Javed E, Scura D, Hala TJ, Seetharam S, Falnikar A, … Lepore AC (2015b). Human iPS cell-derived astrocyte transplants preserve respiratory function after spinal cord injury. Experimental Neurology, 271, 479–492. [PubMed: 26216662]

Li K, Nicaise C, Sannie D, Hala TJ, Javed E, Parker JL, … Lepore AC (2014). Overexpression of the astrocyte glutamate transporter GLT1 exacerbates phrenic motor neuron degeneration, diaphragm compromise, and forelimb motor dysfunction following cervical contusion spinal cord injury. The Journal of Neuroscience, 34, 7622–7638. [PubMed: 24872566]

Luo X, & Park KK (2012). Neuron-intrinsic inhibitors of axon regeneration: PTEN and SOCS3. International Review of Neurobiology, 105, 141–173. [PubMed: 23206599]

Mika J, Zychowska M, Popiolek-Barczyk K, Rojewska E, & Przewlocka B (2013). Importance of glial activation in neuropathic pain. European Journal of Pharmacology, 716, 106–119. [PubMed: 23500198]

Milligan ED, & Watkins LR (2009). Pathological and protective roles of glia in chronic pain. Nature Reviews Neuroscience, 10, 23–36. [PubMed: 19096368]

Nakamura M, & Okano H (2013). Cell transplantation therapies for spinal cord injury focusing on induced pluripotent stem cells. Cell Research, 23, 70–80. [PubMed: 23229514]

Nicaise C, Frank DM, Hala TJ, Authelet M, Pochet R, Adriaens D, … Lepore AC (2013). Early phrenic motor neuron loss and transient respiratory abnormalities after unilateral cervical spinal cord contusion. Journal of Neurotrauma, 30, 1092–1099. [PubMed: 23534670]

Nicaise C, Hala TJ, Frank DM, Parker JL, Authelet M, Leroy K, … Lepore AC (2012a). Phrenic motor neuron degeneration compromises phrenic axonal circuitry and diaphragm activity in a unilateral cervical contusion model of spinal cord injury. Experimental Neurology, 235, 539–552. [PubMed: 22465264]

Nicaise C, Putatunda R, Hala TJ, Regan KA, Frank DM, Brion JP, … Lepore AC (2012b). Degeneration of phrenic motor neurons induces long-term diaphragm deficits following mid-cervical spinal contusion in mice. Journal of Neurotrauma, 29, 2748–2760. [PubMed: 23176637]

Norenberg MD, Smith J, & Marcillo A (2004). The pathology of human spinal cord injury: Defining the problems. Journal of Neurotrauma, 21, 429–440. [PubMed: 15115592]

Ohtake Y, Park D, Abdul-Muneer PM, Li H, Xu B, Sharma K, … Li S (2014). The effect of systemic PTEN antagonist peptides on axon growth and functional recovery after spinal cord injury. Biomaterials, 35, 4610–4626. [PubMed: 24630093]

Pekny M, & Nilsson M (2005). Astrocyte activation and reactive gliosis. Glia, 50, 427–434. [PubMed: 15846805]

Ransohoff RM (2016). A polarizing question: Do M1 and M2 microglia exist? Nature Neuroscience, 19, 987–991. [PubMed: 27459405]

Rao MS, & Mayer-Proschel M (1997). Glial-restricted precursors are derived from multipotent neuroepithelial stem cells. Developmental Biology, 188, 48–63. [PubMed: 9245511]

Rao MS, Noble M, & Mayer-Proschel M (1998). A tripotential glial precursor cell is present in the developing spinal cord. Proceedings of the National Academy of Sciences of the United States of America, 95, 3996–4001. [PubMed: 9520481]

Ristoiu V (2013). Contribution of macrophages to peripheral neuropathic pain pathogenesis. Life Sciences, 93, 870–881. [PubMed: 24140886]

Shanmuganathan K, Gullapalli RP, Zhuo J, & Mirvis SE (2008). Diffusion tensor MR imaging in cervical spine trauma. AJNR. American Journal of Neuroradiology, 29, 655–659. [PubMed: 18238846]

Shih CH, Lacagnina M, Leuer-Bisciotti K, & Proschel C (2014). Astroglial-derived periostin promotes axonal regeneration after spinal cord injury. The Journal of Neuroscience, 34, 2438–2443. [PubMed: 24523534]

Silver J, Schwab ME, & Popovich PG (2015). Central nervous system regenerative failure: Role of oligodendrocytes, astrocytes, and microglia. Cold Spring Harbor Perspectives in Biology, 7, a020602.

Smith GM, Miller RH, & Silver J (1986). Changing role of forebrain astrocytes during development, regenerative failure, and induced regeneration upon transplantation. The Journal of Comparative Neurology, 251, 23–43. [PubMed: 3760257]

Smith GM, Miller RH, & Silver J (1987). Astrocyte transplantation induces callosal regeneration in postnatal acallosal mice. Annals of the New York Academy of Sciences, 495, 185–206. [PubMed: 3474941]

Smith GM, Rutishauser U, Silver J, & Miller RH (1990). Maturation of astrocytes in vitro alters the extent and molecular basis of neurite outgrowth. Developmental Biology, 138, 377–390. [PubMed: 2318341]

Smith GM, & Silver J (1988). Transplantation of immature and mature astrocytes and their effect on scar formation in the lesioned central nervous system. Progress in Brain Research, 78, 353–361. [PubMed: 3247435]

Sofroniew MV (2015). Astrocyte barriers to neurotoxic inflammation. Nature Reviews Neuroscience, 16, 249–263. [PubMed: 25891508]

Strakowski JA, Pease WS, & Johnson EW (2007). Phrenic nerve stimulation in the evaluation of ventilator-dependent individuals with C4- and C5-level spinal cord injury. American Journal of Physical Medicine & Rehabilitation, 86, 153–157.

Warren PM, & Alilain WJ (2014). The challenges of respiratory motor system recovery following cervical spinal cord injury. Progress in Brain Research, 212, 173–220. [PubMed: 25194199]

Warren PM, Awad BI, & Alilain WJ (2014). Drawing breath without the command of effectors: The control of respiration following spinal cord injury. Respiratory Physiology & Neurobiology, 203, 98–108. [PubMed: 25149585]

Zimmer MB, Nantwi K, & Goshgarian HG (2007). Effect of spinal cord injury on the respiratory system: Basic research and current clinical treatment options. The Journal of Spinal Cord Medicine, 30, 319–330. [PubMed: 17853653]

Zukor K, Belin S, Wang C, Keelan N, Wang X, & He Z (2013). Short hairpin RNA against PTEN enhances regenerative growth of corticospinal tract axons after spinal cord injury. The Journal of Neuroscience, 33, 15350–15361. [PubMed: 24068802]

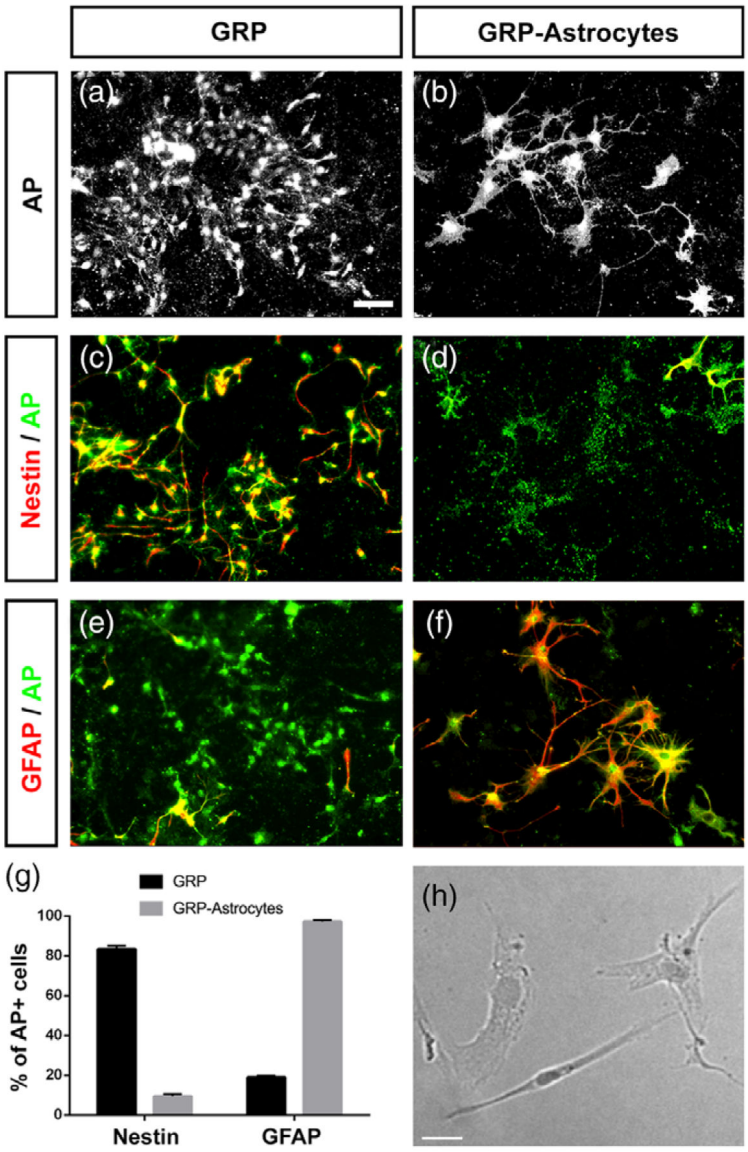

FIGURE 1.

GRPs differentiate into astrocytes in vitro. Undifferentiated AP+ GRPs maintained a glial progenitor-like morphology in culture (a). When stimulated to differentiate into astrocytes, AP+ GRPs acquired an astrocyte-like morphology (b). Prior to astrocyte differentiation, nearly all AP+ cells in the GRP culture expressed nestin (c) but did not express GFAP (e), while differentiated AP+ GRP-derived astrocytes did not express nestin (d) but highly expressed GFAP (f). Quantification of nestin and GFAP expression by AP+ cells (g). Human dermal fibroblasts in culture displayed a fibroblast-like morphology (h). Scale bar: 50 μm

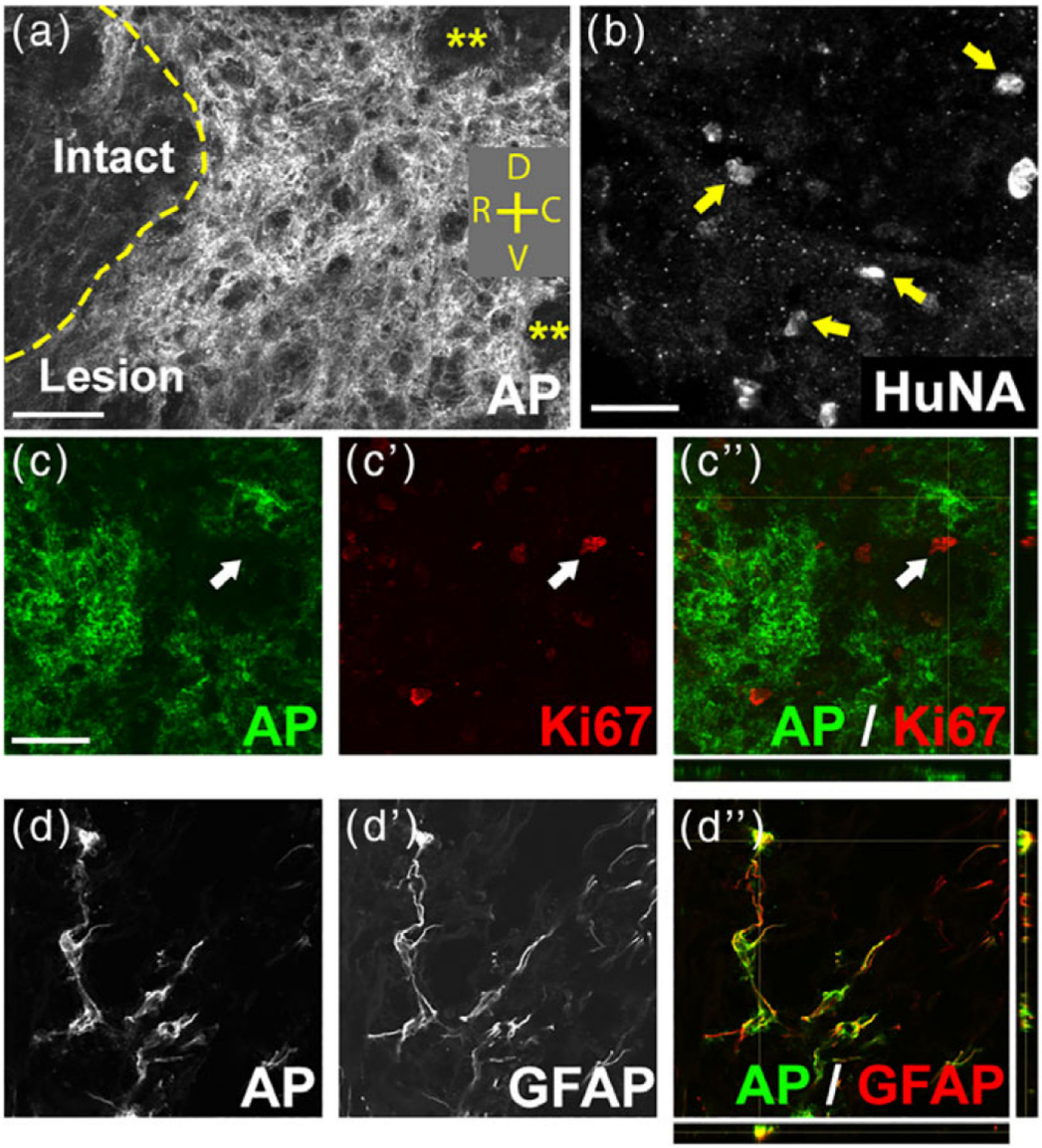

FIGURE 2.

GRP transplants survived long term and efficiently differentiated into astrocytes in the injured spinal cord. AP-labeled GRP-derived cells robustly survived within the lesion site for at least 5 weeks post-transplantation (a). Yellow asterisks in (a) denote areas within the lesion devoid of AP+ cells. Orientation: D = dorsal, V = ventral, R = rostral, C = caudal. HuNA+ fibroblast transplants survived in the lesion site until the 5-week point of sacrifice (b). arrows in (b) denote HuNA+ cells. At 5 weeks post-injection, AP+ cells did not continue to express the proliferation marker Ki67 (c–c"). Arrows in (c–c") denote a Ki67+ cell that was not AP+. The vast majority of AP+ cells at 6 weeks post-transplantation differentiated into GFAP+ astrocytes (d–d"). Scale bar: 50 μm

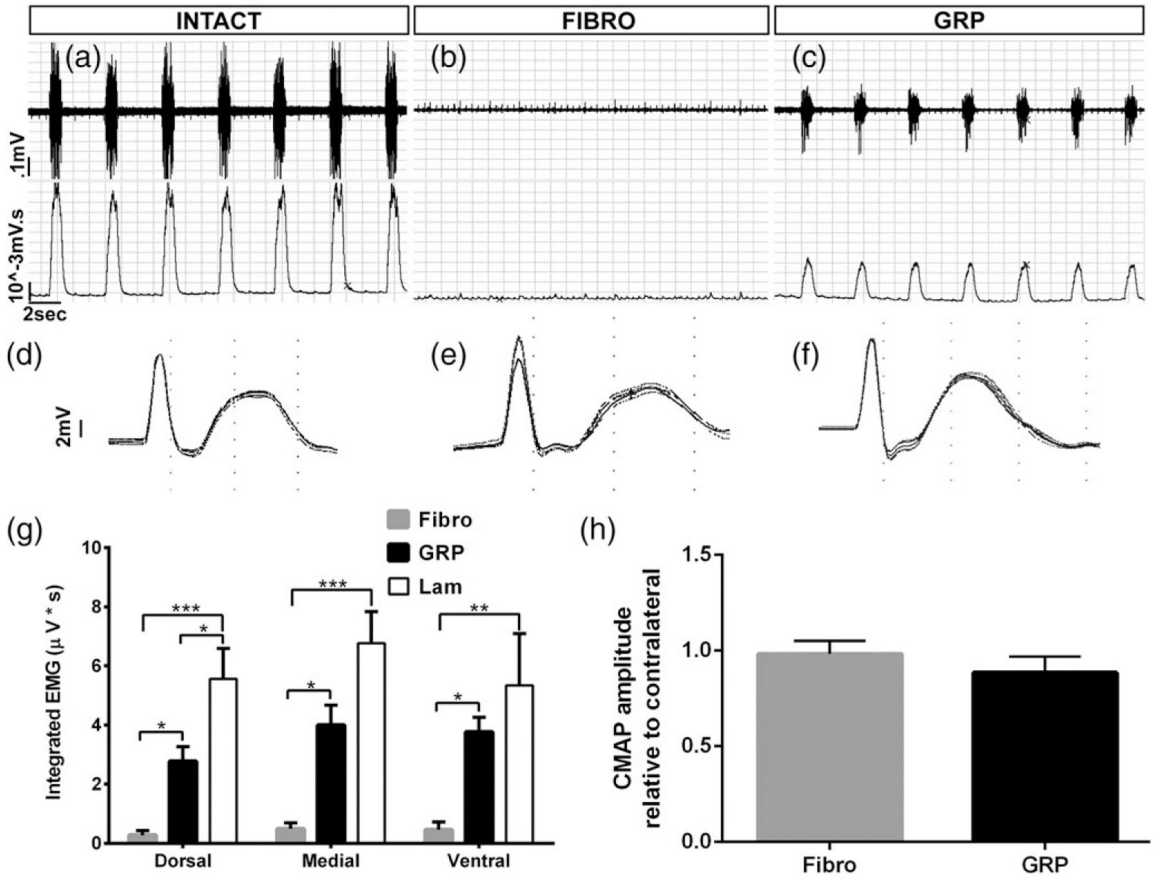

FIGURE 3.

GRP transplantation promoted significant recovery of diaphragm electromyography amplitudes. Compared with control uninjured rats (a), C2 hemisection animals receiving either fibroblast (b) or GRP (c) transplantation showed reduced inspiratory EMG bursts in the hemidiaphragm ipsilateral to SCI. (a,b) Top row shows representative raw EMG traces, while bottom row shows integrated traces. Compared with uninjured controls (d), we did not observe a reduction in diaphragm CMAP amplitudes in C2 hemisection animals receiving either fibroblast (e) or GRP (f) injections. At all three subregions of the hemidiaphragm, GRPs significantly increased EMG burst amplitudes compared with fibroblast control transplants (g). There was no difference in CMAP amplitudes between C2 hemisection animals transplanted with fibroblasts and GRP (h)

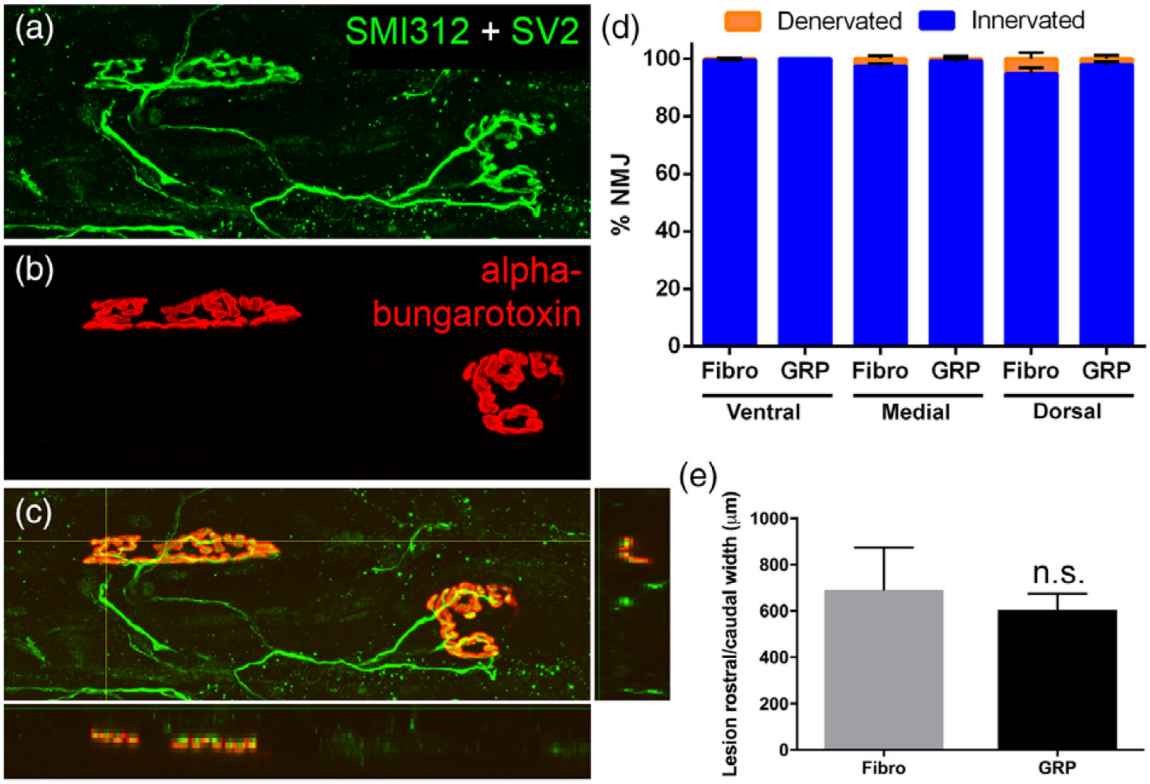

FIGURE 4.

GRPs did not affect lesion size in the cervical spinal cord or morphological innervation at the diaphragm neuromuscular junction. Using whole-mount immunohistochemistry on the ipsilateral hemidiaphragm, we labeled phrenic motor axons all the way to their presynaptic terminals with SMI-312 and SV-2 (a) and postsynaptic nicotinic acetylcholine receptors with Alexa-conjugated α-bungarotoxin (b). Nearly 100% of NMJs at all three muscle sub-regions were completely intact, with compete apposition of the pre-synaptic nerve terminal and the post-synaptic receptors (c). There were no differences in the percentage of innervated and denervated NMJs between fibroblasts and GRPs at any subregion (d). There was no difference between fibroblast and GRP animals in the rostral-to-caudal length of the lesion (e)

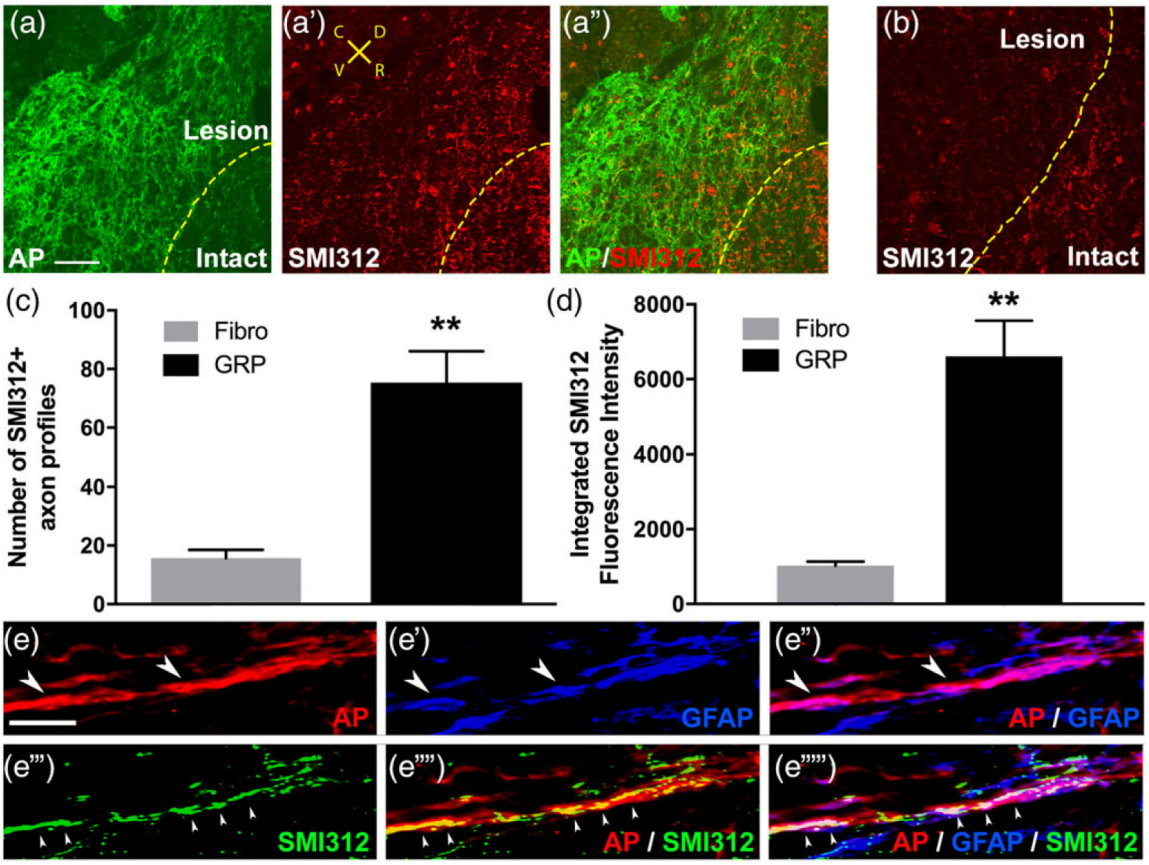

FIGURE 5.

GRPs promoted axonal regeneration. GRPs stimulated significant ingrowth of SMI-312+ axons into the lesion (a–a"). On the contrary, in the control animals that received fibroblast transplantation, a high density of SM1–312+ axons were located in the intact spinal cord directly adjacent to the lesion site; however, we observed almost no growth of SM1–312+ axons across the lesion-intact interface (b). Orientation of all images in panels a–a" and B: D = dorsal, V = ventral, R = rostral, C = caudal. Compared with fibroblasts, GRPs significantly increased both the number of SMI-312+ axons profiles (c) and the density of these SMI-312+ axons (d) within the lesion site. Confocal imaging shows that most of these SMI-312+ fibers in the lesion extended along AP+/GFAP+ cells (e: Red = AP, blue = GFAP, green = SMI-312), demonstrating that axons regenerated along transplant-derived astrocytes within the lesion site. Arrowheads in e"'–e"" denote SMI-312+ host axons growing along AP +/GFAP+ transplant-derived astrocytes. Arrowheads in e–e" denote AP+/GFAP+ transplant-derived astrocytes. Scale bars: 50 μm (a,b), 10 μm (e)

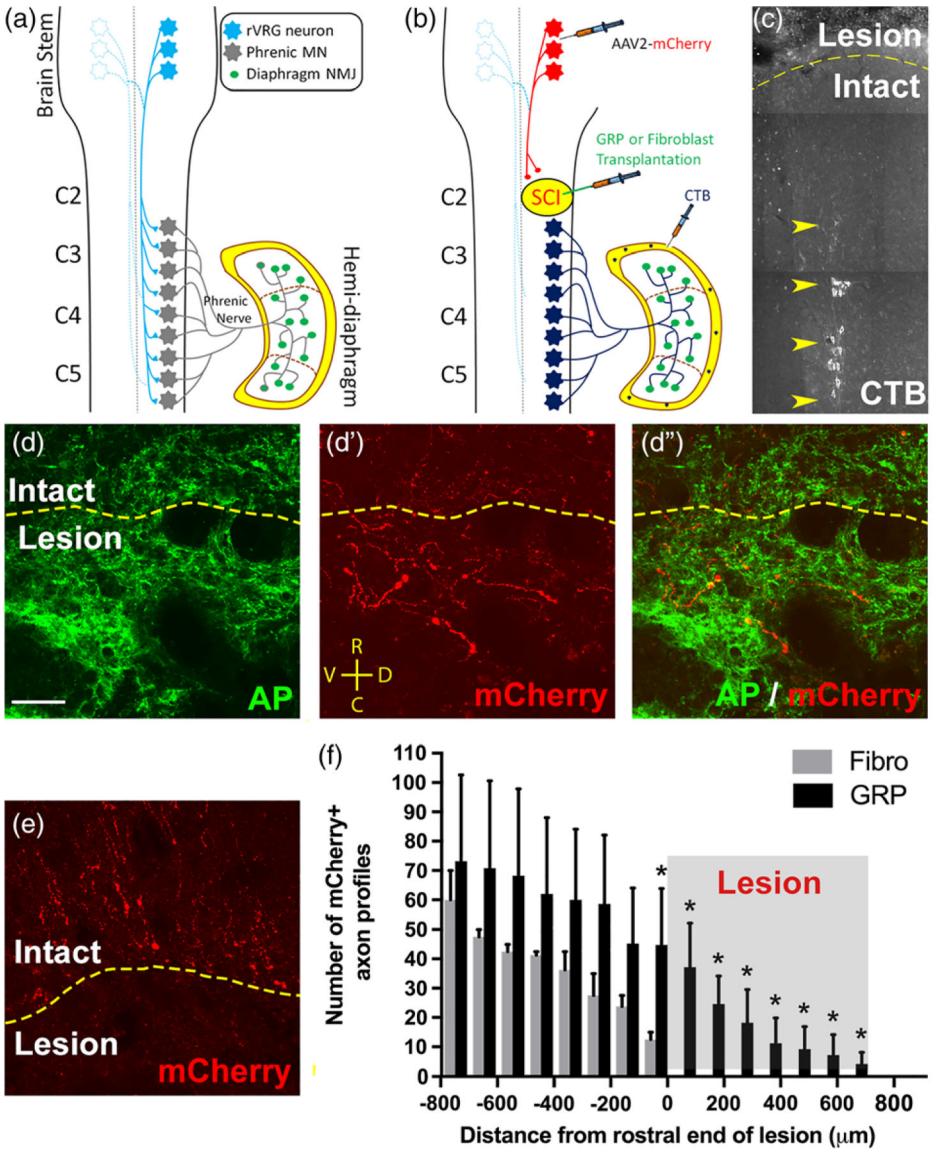

FIGURE 6.

GRPs stimulated robust regeneration of injured rVRG axons, but no synaptic reconnection of these regrowing fibers with PhMNs. Diagram illustrates the intact rVRG-PhMN-diaphragm circuit (a). To label rVRG axons in C2 hemisection rats receiving either GRP or fibroblast transplantation, we stereotaxically injected the anterograde axonal tracer AAV2-mCherry into the ipsilateral rVRG (b). We selectively labeled ipsilateral PhMNs by intrapleurally injecting the retrograde tracer cholera toxin B (b,c). GRPs stimulated robust regeneration of mCherry+ rVRG axons across the rostral intact-lesion border (d–d"). On the contrary, in the control fibroblast animals, all mCherry-labeled rVRG axons stop at the border between the rostral intact spinal cord and the lesion, with many of these axons retracting back from the injury site (e). No rVRG axons regenerate into the lesion site with fibroblast transplantation. Orientation of all images in panels d–d" and e: D = dorsal, V = ventral, R = rostral, C = caudal. Quantification of mCherry+ axon profiles at defined rostral-

caudal distances relative to the rostral end of the lesion (f). GRPs reduced retraction of rVRG axons in the rostral intact spinal and stimulated significant regeneration across the entire lesion site (c). CTB labeling shows that the PhMN pool is located directly caudal to the hemisection (f). scale bar: 50 μm

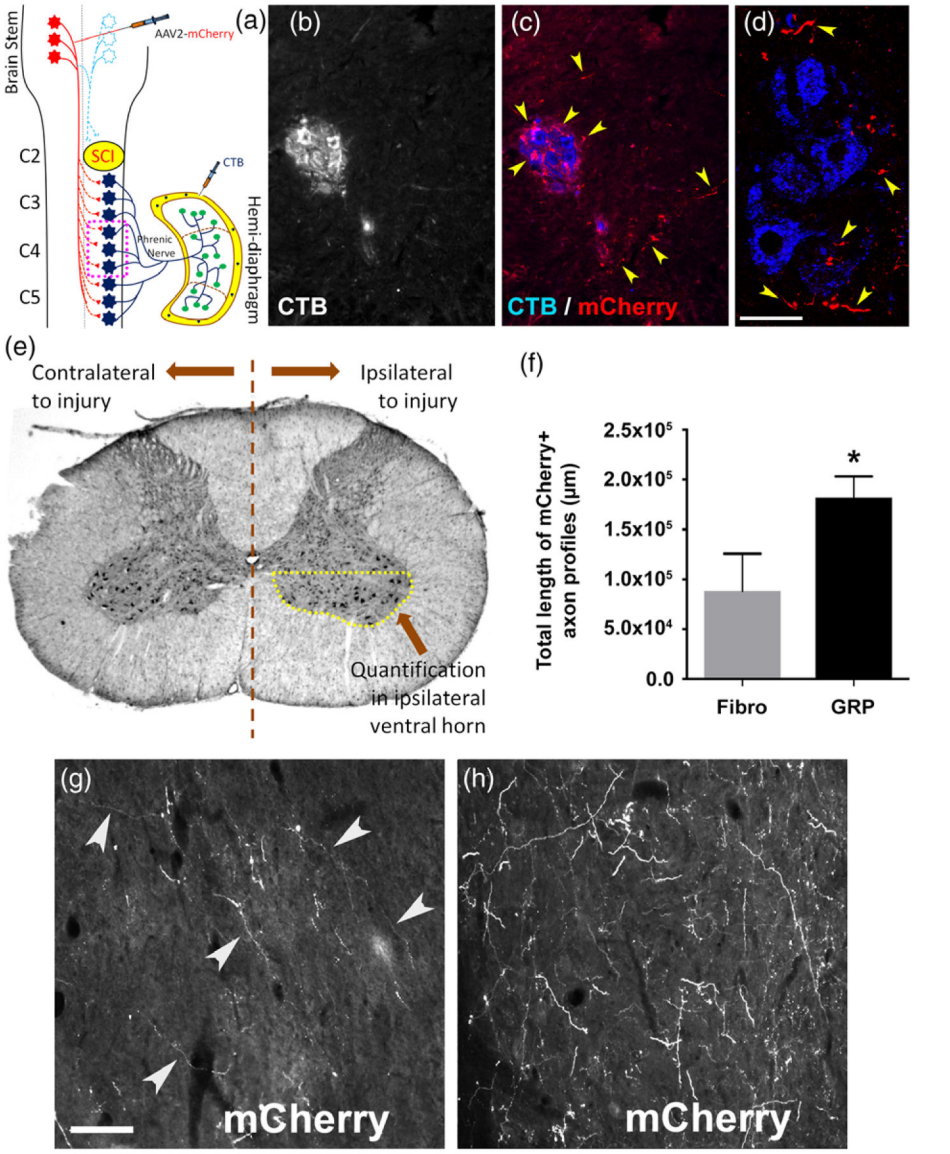

FIGURE 7.

GRPs induced substantial sprouting of spared axons originating in contralateral rVRG. To determine the effects of GRP transplantation on the growth response of spared axons originating in the contralateral rVRG, we injected AAV2-mCherry into the contralateral rVRG in C2 hemisection animals receiving fibroblast or GRP transplantation (a). In the C2 hemisection paradigm, the descending axons originating in the contralateral rVRG are intact and, even in the control C2 hemisection condition, there is some projection of these fibers into the PhMN pool ipsilateral to the injury site (b–d; arrowheads denote mCherry+ rVRG axons). Diagram shows the location of quantification in the ventral horn ipsilateral to the lesion of rVRG axon sprouting (e). We quantified the sprouting of these mCherry-labeled rVRG axons within the C4 ventral horn ipsilateral to the hemisection at 7 weeks post-SCI (f). Compared with fibroblast control (g), GRPs promoted significantly more sprouting of

contralateral rVRG axons within the ipsilateral ventral horn (h). Scale bar: 25 μm (d), 50 μm (g,h)

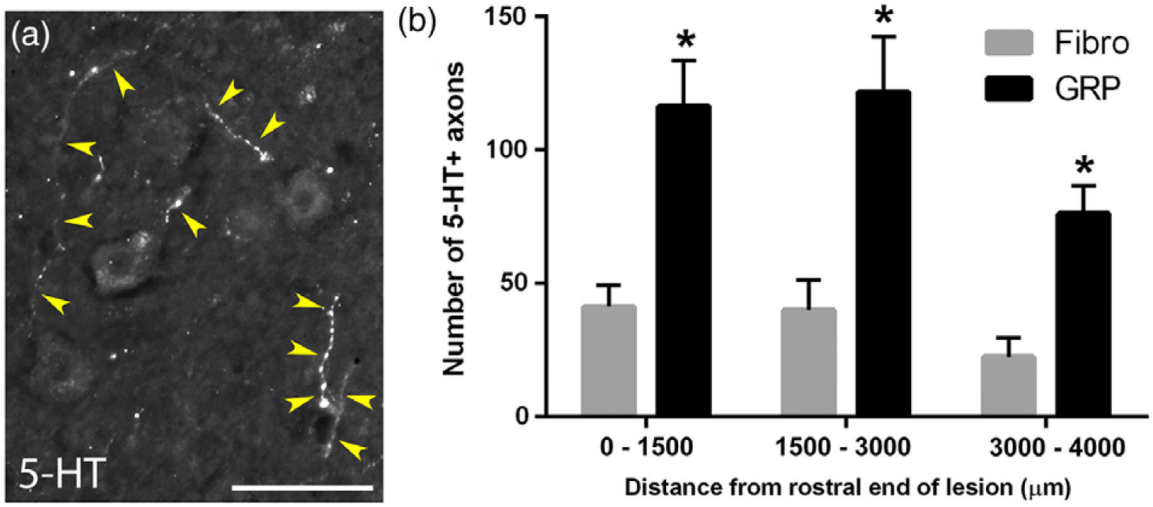

FIGURE 8.

GRPs enhanced 5-HT axon growth within the PhMN pool. We performed 5-HT immunohistochemistry at 5 weeks post-SCI and quantified the numbers of 5-HT axonal profiles surrounding CTB-labeled PhMNs within the ipsilateral ventral horn (a), at the same location as depicted in the schematic in Figure 7. Yellow arrowheads denote 5-HT+ axons. Compared with fibroblast controls, GRP-transplanted animals showed significantly greater numbers of 5-HT axon profiles throughout the PhMN pool at three defined distances from the lesion (b). Scale bar: 25 μm

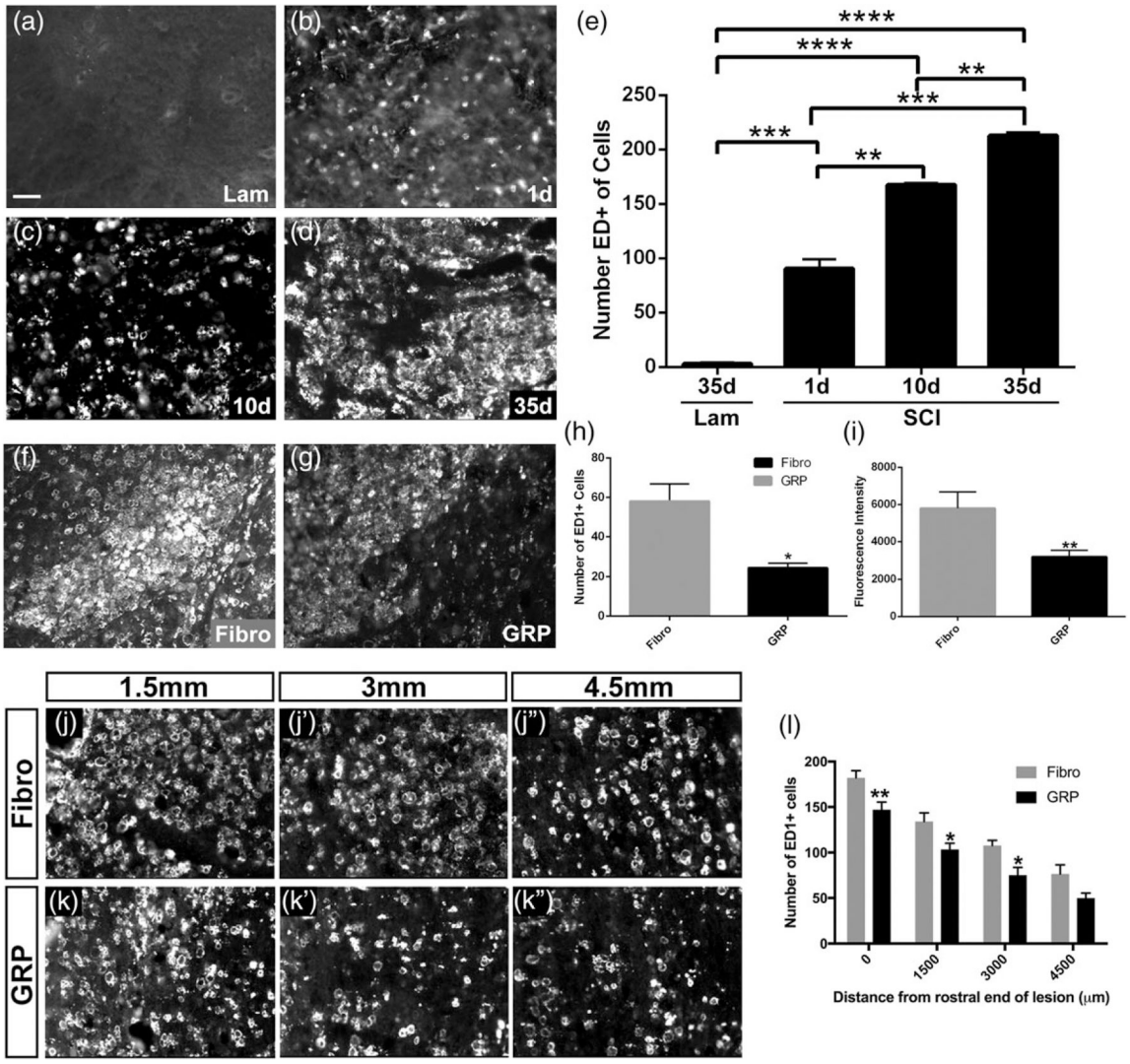

FIGURE 9.

GRPs significantly reduced the macrophage response both within the lesion site and in the intact caudal spinal cord surrounding PhMNs. There were almost no ED1+ cells in the intact C2 spinal cord in laminectomy-only control rats (a). There was a substantial increase in ED1+ cell counts by 1 day posthemisection (b), and these counts progressively increased out to 10 days (c) and 35 days (d) post-SCI (quantification in e). Compared with fibroblasts (f), GRPs (g) significantly reduced the number of ED1+ cells (h) and the intensity of ED1 immunostaining (i) in the lesion site at 5 weeks post-SCI. Compared with fibroblasts (j–j"), GRPs reduced numbers of ED1+ cells in the ipsilateral C3–C5 ventral horn (k–k") at 5 weeks posthemisection (l). Scale bar: 50 μm

TABLE 1

Antibody information

Antibody	Supplier and catalog number	Dilution
Rabbit anti human placental alkaline phosphatase (AP) (H + L)	Adb Serotec (Bio-Rad Laboratories, Hercules, California) Cat# AHP537 (RRID: AB_322551)	1:400
Mouse anti human placental alkaline phosphatase (AP) (H + L)	Novus (Biologicals Centennial, CO) Cat# NB110–3638 (RRID: AB_787958)	1:1,000
Mouse anti nestin (H + L)	Millipore (Sigma Temecula, CA) Cat# MAB353 (RRID: AB_94911)	1:200
Mouse anti glial fibrillary acidic protein(GFAP) (H + L)	R and D systems (Minneapolis, MN) Cat# MAB360 (RRID: AB_2275415)	1:300
Rabbit anti Ki67 (H + L)	Sigma-Aldrich (St. Louis, MO) Cat# SAB4501880 (RRID: AB_10744777)	1:200
Rabbit anti 5-HT (H + L)	Cell sciences (Newburyport, MA) Cat# PA2012 (RRID: AB_170902)	1:15,000
Mouse anti SMI-312 (H + L)	Covance research products Inc (Princeton, NJ) Cat# SMI-312R-100 (RRID:AB_509993)	1:500
Mouse anti EDI (H + L)	Bio-rad Laboratories (Hercules, California) Cat# MCA341GA (RRID: AB_566872)	1:300
Mouse anti human nuclear antigen (HuNA) (H + L)	Millipore (Sigma Temecula, CA) Cat# MAB1281 (RRID: AB_94090)	1:200
Mouse anti NeuN (H + L)	Millipore (Sigma Temecula, CA) Cat# MAB377 (RRID: AB_2298772)	1:200
Mouse anti APC (CC-1) (H + L)	Millipore (Sigma Temecula, CA) Cat# OP80 (RRID: AB_2057371)	1:100